Experimental demonstration of two-dimensional hybrid waveguide-integrated plasmonic crystals on silicon-on-insulator platform

Guanghui Ren, Didit Yudistira, Thach G. Nguyen, Iryna Khodasevych, Steffen Schoenhardt, Kyle J. Berean, Joachim M. Hamm, Ortwin Hess, and Arnan Mitchell

Citation: APL Photonics **2**, 071302 (2017); doi: 10.1063/1.4995996
View online: http://dx.doi.org/10.1063/1.4995996
View Table of Contents: http://aip.scitation.org/toc/app/2/7
Published by the American Institute of Physics

Articles you may be interested in

Exact solution to the steady-state dynamics of a periodically modulated resonator
APL Photonics **2**, 076101 (2017); 10.1063/1.4985381

Nonreciprocity and one-way topological transitions in hyperbolic metamaterials
APL Photonics **2**, 076103 (2017); 10.1063/1.4985064

Interferometric control of the photon-number distribution
APL Photonics **2**, 071301 (2017); 10.1063/1.4992018

Reconfigurable terahertz grating with enhanced transmission of TE polarized light
APL Photonics **2**, 076102 (2017); 10.1063/1.4986505

Ultra-high Q/V hybrid cavity for strong light-matter interaction
APL Photonics **2**, 086101 (2017); 10.1063/1.4994056

Micro-ring resonator quality factor enhancement via an integrated Fabry-Perot cavity
APL Photonics **2**, 056103 (2017); 10.1063/1.4981392

Experimental demonstration of two-dimensional hybrid waveguide-integrated plasmonic crystals on silicon-on-insulator platform

Guanghui Ren,[1,2,a] Didit Yudistira,[1,2] Thach G. Nguyen,[1,2] Iryna Khodasevych,[1,2] Steffen Schoenhardt,[1,2] Kyle J. Berean,[1] Joachim M. Hamm,[3] Ortwin Hess,[3] and Arnan Mitchell[1,2]
[1]*Electronics and Telecommunications Engineering, School of Engineering, RMIT University, Melbourne, VIC 3001, Australia*
[2]*ARC Center for Ultra-high Bandwidth Devices for Optical Systems (CUDOS), RMIT University, Melbourne, VIC 3001, Australia*
[3]*The Blackett Laboratory, Department of Physics, Imperial College London, London SW7 2AZ, United Kingdom*

(Received 31 March 2017; accepted 13 July 2017; published online 26 July 2017)

Nanoscale plasmonic structures can offer unique functionality due to extreme sub-wavelength optical confinement, but the realization of complex plasmonic circuits is hampered by high propagation losses. Hybrid approaches can potentially overcome this limitation, but only few practical approaches based on either single or few element arrays of nanoantennas on dielectric nanowire have been experimentally demonstrated. In this paper, we demonstrate a two dimensional hybrid photonic plasmonic crystal interfaced with a standard silicon photonic platform. Off resonance, we observe low loss propagation through our structure, while on resonance we observe strong propagation suppression and intense concentration of light into a dense lattice of nanoscale hot-spots on the surface providing clear evidence of a hybrid photonic plasmonic crystal bandgap. This fully integrated approach is compatible with established silicon-on-insulator (SOI) fabrication techniques and constitutes a significant step toward harnessing plasmonic functionality within SOI photonic circuits. © *2017 Author(s). All article content, except where otherwise noted, is licensed under a Creative Commons Attribution (CC BY) license (http://creativecommons.org/licenses/by/4.0/).* [http://dx.doi.org/10.1063/1.4995996]

Surface plasmons[1] are coherent oscillations of electrons at metal-dielectric interfaces that can exist either in propagating or in localized forms, i.e., surface plasmon polaritons (SPPs) and localized surface plasmon resonances (LSPRs). The SPPs provide a mechanism for propagating optical photons within extreme sub-wavelength scales, while the LSPRs exhibit extremely large localized electromagnetic fields capable of enhancing optical processes. Through tuning metallic nanostructures, the SPPs and LSPRs on a surface can be easily manipulated, which opens opportunities for their applications on extreme sensitive biosensing,[2,3] superlenses overcoming the diffraction limit,[4,5] nano-focusing light in the gaps between or at the edges of the nanoparticles,[6,7] resonantly transporting energy along particle chains,[8] control of phase[9,10] and polarization,[11] refracting light at negative angles,[9,10] and among others. Most of the work to date, however, is based on interaction with waves incident from free space or via near field optical microscope probes,[12–14] preventing chip-scale integration and limiting the scope of applications to the laboratory. Crucially, to harness the capabilities of plasmonic devices in an integrated photonic circuit, it is necessary to develop platforms where plasmonic surface structures couple to photonic waveguide modes on SOI or III-V semiconductor platforms in ways that do not compromise the characteristics of the photonic modes, i.e., without introducing an unnecessary high propagation loss of distortion of the photonic mode profile.

[a]Electronic mail: guanghui.ren@rmit.edu.au

 © Author(s) 2017

To interface plasmonics with more traditional photonics, hybrid plasmonic photonic waveguides have been proposed,[15–22] which has a dielectric buffer layer to control the coupling between photonic and plasmonic modes. By using the proposed hybrid plasmonic waveguides, Février[17] and Apuzzo[18] experimentally realized a hybrid integration of gold nano-particles chain on silicon chip and characterized their interactions among each element through near field scanning, respectively. Most recently, Luo[19] realized nanofocusing in a hybrid plasmonic photonic nanotaper structure. However, each of these demonstrations interfaces to a single element or short one dimensional chains of elements, providing limited opportunity for sophisticated photonics such as bandgap engineering and electromagnetic crystal structures which have been so successful in dielectric photonics, particularly for intense concentration of light combined with dispersion engineering leading to enormous enhancements in nonlinearity.[23,24] In order to achieve electromagnetic crystal functionality in a hybrid plasmonic-photonic structure one would require a relatively large array of elements with sufficiently low-loss propagation between the elements such that strong resonances could be formed due to multiple reflections.[1] Also, to warrant the hybridizing plasmonics and photonics, it would be important to maintain the deeply sub-wavelength optical confinement characteristic of nanoplasmonics.

In this work, we present plasmonic nanogap tilings[20] on a readily available SOI chip. We harness integrated silicon photonic lenses and grating couplers[25] to launch and collect collimated transverse electric (TE) beam to interact with nanogap tilings. The stop band of the practically realized hybrid waveguide-integrated plasmonic crystals on SOI platform is experimentally characterized and theoretically analysed providing proof of the silicon photonic plasmonic crystal. Using transmission scanning near field optical microscopy (Tra-SNOM)[26,27] to directly and simultaneously measure the nanogap tilings, we find that the optical fields concentrate in the sub-wavelength gaps of the nanoplasmonic surface tiling. We thus prove that nanoscale plasmonic confinement and distributed electromagnetic crystal resonance can be achieved simultaneously.

The schematic representations and the top and cross-section views of the hybrid waveguide-integrated plasmonic crystals on SOI platform are shown in Figs. 1(a) and 1(b). The silicon photonic plasmonic crystal consists of 26 periods of 30 nm thick silver triangular-latticed nanogap tiling along optical axis on a silicon slab waveguide with a 30 nm thin SiO_2 isolation layer between them. The silver nanogap tiling introduces periodic perturbation on the evanescent field of the guided TE mode in the silicon slab beneath. The input port of the device consists of a grating coupler which couples TE light into the chip from a single mode fibre and an input optical lens, with the radius of 100 μm and the focal length of 395 μm which collimates the injected mode into a 28 μm wide (measured at 1/e) Gaussian beam.[25] The output port, similarly, consists of an output optical lens which collects the light from silicon photonic plasmonic crystal and focuses onto the output grating coupler which couples light from the chip to an output single mode optical fibre. Figure 1(b) shows the scanning electron microscopy (SEM) image of the two-dimensional plasmonic crystal device integrated on the SOI platform with pitch length (L) equals to 330 nm while the gap between adjacent triangles is $G = L/10 = 33$ nm.

According to theoretical predictions,[20] the TE slab mode should be used to excite the nanogap tilings structure. The evanescent field of the TE dielectric mode confined in the planar silicon slab waveguide interacts with the silver plasmonic crystal through SiO_2 buffer layer to excite LSPRs in corners of C_{3v} trimer molecules.[27] When the trimer molecules are coupled in dense arrays, the LSPRs strongly couple to the plasmonic band that can support the propagation of SPPs along the nanoparticles chain.[8] If the propagating plasmonic and photonic modes are phase matched, mutual coupling occurs which leads to the formation of hybrid waveguide-plasmon polaritons.[15] When this coupling become resonant, the propagation of energy is prevented, i.e., the transmission stop band is formed.

In order to theoretically investigate the band structure of the silicon photonic plasmonic crystal, a full-wave finite element method (see supplementary material and Ref. 20) is used. Figure 2(a) shows the band structure of the silicon photonic plasmonic crystal for TE-like mode along the Γ-M direction with the transmission stop band marked in light green. Figure 2(b) shows the top-view and cross-section view of the energy distribution for hybrid modes in a unit cell at position "A" on the lower stop band edge in Fig. 2(a), and the plots for hybrid modes at different positions on stop band edges can be found in supplementary material. It can be seen from Fig. 2(b) that the optical fields are

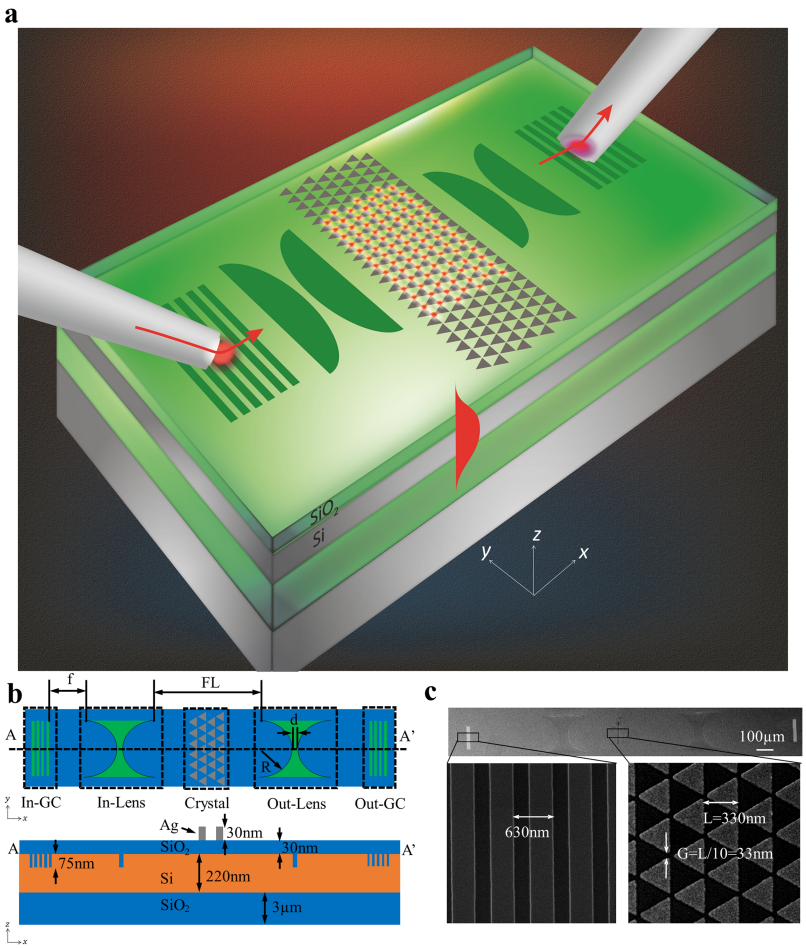

FIG. 1. (a) Schematic representations of the coupling between optical and plasmonic elements and the coupling between the chip and optical fibers. (b) Illustrations of the two-dimensional hybrid waveguide-integrated plasmonic crystals on SOI platform and the cross-section view along the dashed line AA'. Two dimensional array of 30 nm thick triangle silver patches arranged in a triangular lattice integrated on SOI platform with 220 nm silicon layer and 3 μm buried silicon dioxide layer, isolated by 30 nm layer of SiO_2. The device consists of an input grating coupler (In-GC) which couples TE light from a single mode fiber into a slab waveguide, which is then collimated by an input optical lens (In-Lens) before impinging the silicon photonic plasmonic crystals. An output optical lens (Out-Lens) collects the beam passing through the crystal and focuses the beam onto the output grating coupler (Out-GC), which is then picked up by an output single mode optical fibre. The optical lens is composed of two semi-disk with radius R = 100 μm and separation d = 50 μm. The separation (f = 296 μm) between the grating coupler and the optical lens is determined by the focal length of the optical lens.[25] The separation (FL) between input and output optical lenses is set to be 500 μm. (c) SEM image of the fabricated device with the plasmonic crystal with the pitch length, L = 330 nm, and the gap between the adjacent triangles, G = L/10 = 33 nm, and the grating coupler with the period of 630 nm and the filling factor of 60%.

concentrated at triangle corners in the air and are much stronger than those in the silicon waveguide ones as expected, indicating the hybrid modes are excited through coupling from TE-like modes in the silicon waveguide underneath.

For modeling the structures, the stop band was simulated while varying pitch length as a continuous variable. Experimentally the pitch length must be fixed for each realized device, with the excitation wavelength being used as a continuous variable. The relationship between pitch length and wavelength stop bands is shown in supplementary material. Devices are fabricated using electron-beam-lithography (EBL), with details in the supplementary material. The measured transmission of a systematic set of silicon photonic plasmonic crystals is presented in Fig. 2(c). The vertical axis represents the total loss for the device, including all input and output fibers connection losses, the polarization controller loss, and grating coupler losses (about 4.5 dB/facet) which can be estimated at around 15 dB.[25] Off resonance the attenuation of the silicon photonic plasmonic crystal is only

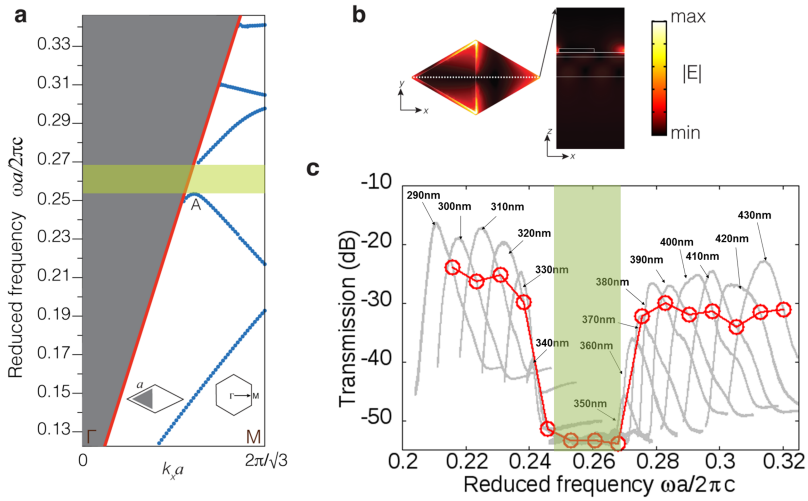

FIG. 2. Silicon photonic plasmonic crystals band structure characteristics. (a) Calculated band structure of the silicon photonic plasmonic crystal with lattice constant $a = 2L/\sqrt{3}$ for TE-like mode along the Γ-M (k_x) direction as indicated by the inset. Hybrid TE-like guided modes are under the light line (red solid line), which corresponds to the dispersion of SiO_2. (b) Calculated hybrid TE-like guided mode profile at the position in the band structure, which is indicated by "A" in (a), showing a strong localization of optical field within the triangle corners. (c) Measured transmission spectra, with typical grating couplers response, of the silicon photonic plasmonic crystal at different pitch lengths, ranging from 290 nm to 430 nm, which shows suppression of TE propagating mode at reduced frequency of around 0.26 as indicated by the shaded area, which is in good agreement with the calculated band structure in (a), providing evidence of the existence of photonic bandgap. The red dashed line represents the transmission spectrum at wavelength 1550 nm for different pitch lengths.

1-2 dB supporting the claim that this structure can achieve low loss. The horizontal axis is the reduced frequency including both wavelength and pitch length of the structure. Due to the limited frequency range of the tunable laser used in this experiment, it is impossible to observe the complete stop band for a device with a specific pitch length. Hence 15 different devices with pitch length varying from 290 to 430 nm in the step of 10 nm are used to characterize the complete transmission stop band (the response at 1550 nm is highlighted with circles). These experimental results are in excellent agreement with the theoretical predictions in Fig. 2(a).

Following the simulation results of Fig. 2(b) and those predicted in Ref. 20, strong confinement of electromagnetic field at the triangle corners is expected to occur at a frequency in the vicinity of the edge of the stop band. The simulated field enhancement on the stop band edge is more than 5–10 times stronger than those near stop band and passband in Ref. 20. Therefore, for near field optical microscopy characterization, we fabricated and then packaged (see supplementary material for more details) a device with pitch length L = 330 nm as it mostly covers the lower part of the edge of the stop band [see Fig. 3(a)]. We measured the near field properties at different frequencies, 0.235, 0.236, 0.238, and 0.240, and the results are shown in Figs. 3(c)–3(f); Fig. 3(b) shows the corresponding device topography and the light is excited from left side and collected from the right side. We can see in Figs. 3(c)–3(f) that as we increase the frequency the electromagnetic field increases and reaches maximum at around 0.236, which then drops quickly at 0.240. As expected, the field is strongly confined at the triangular corners [see the inset of Fig. 3(e) for comparison with the simulation]. We also found from Figs. 3(c)–3(f) that the plasmonic crystal are spatially non-uniformly excited and they follow a periodicity along the optical axis, which are due to the periodic coupling of the propagating light between plasmonic crystals and the silicon waveguide, as investigated in Ref. 28. A near-field simulation result showing such phenomenon for L = 330 nm at reduced frequency 0.238 can be found in supplementary material. To qualitatively shows the optical field enhancement in the plasmonic crystals, we plot in Fig. 4 the averaged intensity, calculated from over 150 silver triangles in the dashed area in the inset, as a function of frequency (red filled circle), superimposed on the measured transmission spectrum (blue dashed line). We can see on Fig. 4 that the frequency 0.236 sits right at the stop band edge, which renders a strong field intensity due to the resonant coupling between dielectric modes and plasmonic modes as previously observed, whereas 0.235 lies in the

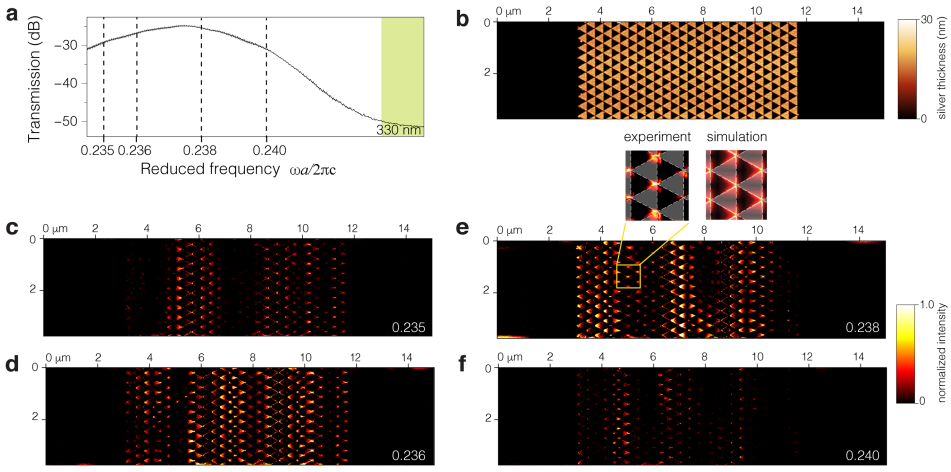

FIG. 3. Observation of near-field properties of a silicon photonic plasmonic crystal with pitch length L = 330 nm. (a) Measured transmission spectrum for the silicon photonic plasmonic crystal. (b) The topography of the silicon photonic plasmonic crystal. (c)-(f) The measured near-field results for the silicon photonic plasmonic crystal device at reduced frequency 0.235, 0.236, 0.238, and 0.240, respectively. The inset in (e) represents the comparison between simulated and measured near-field results.

passband and 0.238 and 0.240 are very close to the stop band, which have lower field confinement. Although 0.235 sits in the passband and the coupling between dielectric and plasmonic modes are off-resonance, there is still optical field enhancement on the triangle corners, which is due to the lightning rod effect[29] of silver triangles that can lead to a concentration of field strength into the focal points.

In summary we have presented the first experimental demonstration of silicon photonic plasmonic crystal which combines engineered electromagnetic crystal resonant bandgap behaviour with nanoscale plasmonic sub-wavelength confinement at optical frequencies on a standard silicon photonic platform suitable for mass fabrication. We have shown the silicon photonic plasmonic crystal bandgap behaviour and intense field concentration in the nano-gaps at the edges of the stop band. This demonstration opens a new frontier for integrated plasmonics surface crystals which combines dispersion engineering electromagnetic crystals with the nanoscale optical confinement that can be achieved with plasmonic structures. Using this platform arbitrary surface elements and crystal structures can be realized with relative ease. Further, with field hot-spots on the surface, it becomes possible to functionalize these structures to conduct spectroscopy or study strong light-matter interaction on

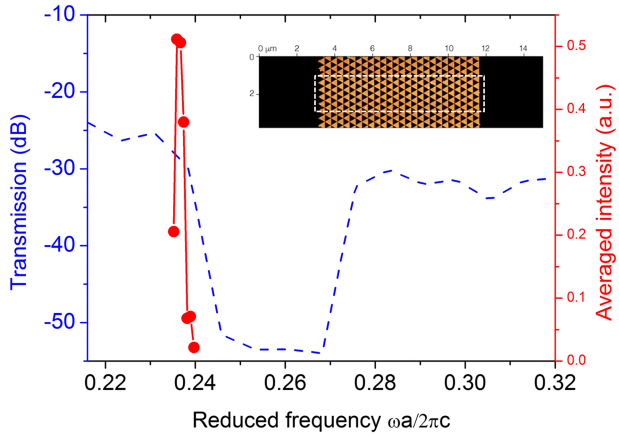

FIG. 4. Measured averaged near-field optical intensity at different frequencies (red line) and the transmission spectrum (blue line) for a silicon photonic plasmonic crystal with pitch length L = 330 nm. The dashed area shown in the inset is used to calculate the average intensity.

a chip, for example, with nanoscale materials such as quantum dots providing a route for integrated, on-chip quantum optics and molecular scale biosensing.

See supplementary material for the simulation method, fabrication method, transform from pitch length spectrum to wavelength spectrum, near-field simulation results, transmission spectrum measurement setup, and Tra-SNOM measurement setup.

This work is supported by Australian Research Council's Discovery project (No. DP1096153) and the ARC Centre of Excellence CUDOS (No. CE110001018). This work is performed in part at the Melbourne Centre for Nanofabrication (MCN), RMIT Micronano research facility (MNRF) in the Victorian Node of the Australian National Fabrication Facility (ANFF), and RMIT microscopy and microanalysis facility (RMMF).

[1] W. L. Barnes, A. Dereux, and T. W. Ebbesen, Nature **424**, 824 (2003).
[2] J. N. Anker, W. P. Hall, O. Lyandres, N. C. Shah, J. Zhao, and R. P. Van Duyne, Nat. Mater. **7**, 442 (2008).
[3] K. V. Sreekanth, Y. Alapan, M. ElKabbash, E. Ilker, M. Hinczewski, U. A. Gurkan, A. De Luca, and G. Strangi, Nat. Mater. **15**, 621 (2016).
[4] N. Fang, H. Lee, C. Sun, and X. Zhang, Science **308**, 534 (2005).
[5] Z. Liu, H. Lee, Y. Xiong, C. Sun, and X. Zhang, Science **315**, 1686 (2007).
[6] V. G. Kravets, F. Schedin, A. V. Kabashin, and A. N. Grigorenko, Opt. Lett. **35**, 956 (2010).
[7] W. Zhou and T. W. Odom, Nat. Nanotechnol. **6**, 423 (2011).
[8] S. A. Maier, P. G. Kik, H. A. Atwater, S. Meltzer, E. Harel, B. E. Koel, and A. A. G. Requicha, Nat. Mater. **2**, 229 (2003).
[9] N. Yu, P. Genevet, M. A. Kats, F. Aieta, J.-P. Tetienne, F. Capasso, and Z. Gaburro, Science **334**, 333 (2011).
[10] X. Ni, N. K. Emani, A. V. Kildishev, A. Boltasseva, V. M. Shalaev, V. G. Veselago, J. B. Pendry, Z. Liu, H. Lee, Y. Xiong, C. Sun, X. Zhang, J. B. Pendry, D. Schurig, D. R. Smith, and N. Yu, Science **335**, 427 (2012).
[11] J. Lin, J. P. B. Mueller, Q. Wang, G. Yuan, N. Antoniou, X.-C. Yuan, and F. Capasso, Science **340**, 331 (2013).
[12] B. Hecht, H. Bielefeldt, L. Novotny, Y. Inouye, and D. Pohl, Phys. Rev. Lett. **77**, 1889 (1996).
[13] J. R. Krenn, B. Lamprecht, H. Ditlbacher, G. Schider, M. Salerno, A. Leitner, and F. R. Aussenegg, Europhys. Lett. **60**, 663 (2002).
[14] M. Brun, A. Drezet, H. Mariette, N. Chevalier, J. C. Woehl, and S. Huant, Europhys. Lett. **64**, 634 (2003).
[15] A. Christ, S. G. Tikhodeev, N. A. Gippius, J. Kuhl, and H. Giessen, Phys. Rev. Lett. **91**, 183901 (2003).
[16] F. Bernal Arango, A. Kwadrin, and A. F. Koenderink, ACS Nano **6**, 10156 (2012).
[17] M. Février, P. Gogol, G. Barbillon, A. Aassime, R. Mégy, B. Bartenlian, J.-M. Lourtioz, and B. Dagens, Opt. Express **20**, 17403 (2012).
[18] A. Apuzzo, M. Février, R. Salas-Montiel, A. Bruyant, A. Chelnokov, G. Lérondel, B. Dagens, and S. Blaize, Nano Lett. **13**, 1000 (2013).
[19] Y. Luo, M. Chamanzar, A. Apuzzo, R. Salas-Montiel, K. N. Nguyen, S. Blaize, and A. Adibi, Nano Lett. **15**, 849 (2015).
[20] P. M. Z. Davies, J. M. Hamm, Y. Sonnefraud, S. A. Maier, and O. Hess, ACS Nano **7**, 7093 (2013).
[21] R. F. Oulton, V. J. Sorger, D. A. Genov, D. F. P. Pile, and X. Zhang, Nat. Photonics **2**, 496 (2008).
[22] D. Dai and S. He, Opt. Express **17**, 16646 (2009).
[23] Y. Akahane, T. Asano, B. Song, and S. Noda, Nature **425**, 944 (2003).
[24] M. Soljačić and J. D. Joannopoulos, Nat. Mater. **3**, 211 (2004).
[25] G. Ren, T. G. Nguyen, and A. Mitchell, IEEE Photonics Technol. Lett. **26**, 1438 (2014).
[26] J. T. Robinson, S. F. Preble, and M. Lipson, Opt. Express **14**, 10588 (2006).
[27] R. Salas-Montiel, A. Apuzzo, C. Delacour, Z. Sedaghat, A. Bruyant, P. Grosse, A. Chelnokov, G. Lerondel, and S. Blaize, Appl. Phys. Lett. **100**, 231109 (2012).
[28] M. Février, P. Gogol, A. Aassime, A. Chelnokov, A. Apuzzo, S. Blaize, and J. Lourtioz, Nano Lett. **12**, 1032 (2012).
[29] J. Gersten and A. Nitzan, J. Chem. Phys. **73**, 3023 (1980).